A sequence in the carboxy-terminus of the α_{1C} subunit important for targeting, conductance and open probability of L-type Ca^{2+} channels

Klaus J.F. Kepplinger[a], Heike Kahr[a], Günter Förstner[a], Max Sonnleitner[a], Hansgeorg Schindler[a], Thomas Schmidt[b], Klaus Groschner[c], Nikolai M. Soldatov[d], Christoph Romanin[a,*]

[a] *Institute for Biophysics, University of Linz, Altenbergerstr. 69, A-4040 Linz, Austria*
[b] *Department of Biophysics, Leiden University, Leiden, The Netherlands*
[c] *Institute of Pharmacology and Toxicology, University of Graz, A-8010 Graz, Austria*
[d] *National Institute on Aging, NIH, Baltimore, MD 21224-6825, USA*

Received 12 June 2000

Edited by Maurice Montal

Abstract The role of the 80-amino acid motif 1572–1651 in the C-terminal tail of α_{1C} Ca^{2+} channel subunits was studied by comparing properties of the conventional $\alpha_{1C,77}$ channel expressed in HEK-tsA201 cells to three isoforms carrying alterations in this motif. Replacement of amino acids 1572–1651 in $\alpha_{1C,77}$ with 81 non-identical residues leading to $\alpha_{1C,86}$ impaired membrane targeting and cluster formation of the channel. Similar to $\alpha_{1C,86}$, substitution of its 1572–1598 ($\alpha_{1C,77L}$) or 1595–1652 ($\alpha_{1C,77K}$) segments into the $\alpha_{1C,77}$ channel yielded single-channel Ba^{2+} currents with increased inactivation, reduced open probability and unitary conductance, when compared to the $\alpha_{1C,77}$ channel. Thus, the C-terminal sequence 1572–1651 of the α_{1C} subunit is important for membrane targeting, permeation and open probability of L-type Ca^{2+} channels.

Key words: Class C-type Ca^{2+} channel; Carboxyl tail; Targeting; Conductance; Inactivation; Fluorescence microscopy; GFP-labeled α_{1C} subunit

1. Introduction

The voltage-gated L-type Ca^{2+} channel is an essential part of signal transduction systems in many cell types, triggering essential processes, such as muscle contraction [1,2] or neuronal gene expression [3–6]. It is composed of the pore-forming α_{1C} subunit and auxiliary β- and $\alpha_2\delta$-subunits [7,8]. The carboxy-terminus of the α_{1C} subunit has attracted much attention [9–11] because of its potential involvement in channel gating. Two human splice variants of the principal 2138-amino acids pore-forming α_{1C} subunit, $\alpha_{1C,77}$ and $\alpha_{1C,86}$, differ in their carboxy-terminal tail sequence by 80 amino acid residues in positions 1572–1651 (Table 1; [12,13]). When expressed in oocytes, these two channel splice variants exhibit strong differences in inactivation properties [10]. Whole-cell Ba^{2+} currents of the $\alpha_{1C,86}$ channel inactivate significantly faster than those through $\alpha_{1C,77}$. Furthermore, with Ca^{2+} as charge carrier, inactivation of the current through $\alpha_{1C,77}$ is greatly accelerated in contrast to the $\alpha_{1C,86}$ inactivation which is essentially Ca^{2+}-independent. Two independent determinants for Ca^{2+}-induced inactivation were identified within this sequence by segment exchange analysis [11], one located in the L-motif (1572–1598) and the other in the K-motif (1595–1651) (Table 1). A calmodulin binding IQ region (1624–1635) within the K-motif has been shown to be important for Ca^{2+}-dependent inactivation [14–16].

To further analyze the role of amino acids 1572–1651 in the regulation of Ca^{2+} channel activity, we studied here expression, subcellular localization as well as electrophysiological properties of the $\alpha_{1C,77}$ and $\alpha_{1C,86}$ channels and of two derived segmental mutants $\alpha_{1C,77K}$ and $\alpha_{1C,77L}$ (Table 1; [11]) in the HEK-tsA201 mammalian expression system. The results of our study indicate that the sequence 1572–1651 in the carboxy-terminal tail of the α_{1C} subunit determines not only channel inactivation, but also membrane targeting, single-channel conductance and open probability of L-type Ca^{2+} channels.

2. Materials and methods

2.1. Materials

EGFP was purchased from Clontech (Heidelberg, Germany). The cDNA of the CD8 receptor (EBO pcD Leu2) was kindly provided by Richard Horn (Thomas Jefferson University Medical School, Philadelphia, PA, USA). The cDNA of the fusion construct of EGFP and the pleckstrin homology domain of phospholipase C δ1 (EGFP-PH) was a gift from Tobias Meyer (Durham, North Carolina, USA). Tissue culture media and reagents were purchased from Life Technology, Vienna, Austria. (−)-BAYK 8644 was from Research Biochemical International, Vienna, Austria and all other chemicals from Sigma, Vienna, Austria. Magnetic beads carrying antibodies against the CD8 receptor were purchased from Dynal, Hamburg, Germany.

2.2. Molecular biology

2.2.1. Preparation of eukaryotic expression plasmids encoding the α_{1C} channel isoforms. 77pcDNA3 coding for $\alpha_{1C,77}$ [17] used for eukaryotic transfection was inserted into plasmid pcDNA3 (Invitrogen) and contained the Kozak consensus sequence (5′-ccgcca-3′) upstream of the initiation codon. 86pcDNA3 was prepared by replacing the *Sfu*I (3341)–*Aat*II (5494) fragment of pHLCC77 with the corresponding fragment [10]. To prepare 77KpcDNA3 and 77LpcDNA3, the pHLCC77K and pHLCC77L plasmids [11], respectively, were digested with *Bam*HI, blunt-ended using the Klenow DNA polymerase, digested with *Ppu*MI (2760) and the obtained 3′-terminal 3.9-kb fragments were ligated into 77pcDNA3 to replace the corresponding fragment in the *Ppu*MI (2760)/*Not*I (blunt-ended) cassette.

2.2.2. Construction of the 5′-GFP-labeled $\alpha_{1C,77}$ and $\alpha_{1C,86}$. A 5′-terminal *Hin*dIII linker upstream Kozak sequence and 3′-terminal *Bgl*II linker were incorporated into the flanking regions of the open reading frame of the pGreen Lantern-1 DNA (Life Technology, Gai-

*Corresponding author. Fax: (43)-732-2468 9280.
E-mail: christoph.romanin@jk.uni-linz.ac.at

0014-5793/00/$20.00
PII: S0014-5793(00)01791-9

thersburg, MD, USA) ORF by PCR using sense 5′-aaagcttgccgccaccatgag-3′ and antisense 5′-agatctcttgtacagctcgtcc-3′ primers, respectively. The *Hin*dIII/*Bgl*II pGreen Lantern-1 cassette was ligated into the 77pcDNA3 vector at *Hin*dIII/*Bam*HI sites so that the 5′-GFP-77pcDNA3 construct encoded the enhanced GFP fused to $\alpha_{1C,77}$ via RSAT tetrapeptide. 5′-GFP-86pcDNA3 was prepared by replacing the 3.9-kb *Ppu*MI/*Not*I fragment of 5′-GFP-77pcDNA3 with the respective fragment of pHLCC86B.

Nucleotide sequences of all PCR products, as well as ligation sites were verified using the ABI Prism™ Dye Terminator Cycle Sequencing Kit with AmpliTaq DNA Polymerase (Perkin-Elmer, Norwalk, USA).

2.3. Cell culture and transfection of tsA201 cells

tsA201 cells were cultured in DMEM medium supplemented with streptomycin (100 μg/ml)/penicillin (100 U/ml) and 10% FCS in a humidified atmosphere (95%) at 5% CO_2 and 37°C. Cells were used for 12–14 passages and were passed every 4 days. Transfection was performed using SuperFect (Qiagen, Hilden, Germany). In brief, cells exhibiting confluence of about 30–50% were transfected with 2.5 μg of total cDNA (molar ratio of α_{1C}:β_{2a}:$\alpha_2\delta$:EGFP:CD8 = 1:1.6:1.4:2.5:0.7). Transfection efficiency was estimated by the fraction of cells showing EGFP fluorescence, and was in the range of 20–60%. Expression of CD8 receptor and binding of CD8 antibody-coated beads (Dynal) was used as visual marker to identify cells in electrophysiological experiments. Binding of the beads (range 3–15 per cell) was estimated to occur in 1–5% of the total number of cells.

2.4. Microscopy

Cells transfected with α_{1C} constructs carrying green fluorescent protein (GFP) at their amino-terminus were imaged either by conventional fluorescence microscopy or by two-photon confocal fluorescence microscopy [18]. Conventional fluorescence microscopy was performed on an inverted microscope (Axiovert 100TV, Zeiss, Oberkochen, Germany) equipped with a 100× NA 1.3 objective (Zeiss) and a Sensicam slow scan CCD camera (PCO CCD Imaging, Kellheim, Germany). In confocal microscopy, cover slips carrying the cells were mounted onto a piezo-driven scanning stage (PI, Waldbronn, Germany) on an inverted microscope (AxioVertS 100TV, Zeiss) equipped with a 100× NA1.3 objective (Zeiss). The size of the point-spread function was measured to be 0.25 μm in lateral and 0.8 μm in axial direction. The fluorescence was excited by the light from a fs-Ti:sapphire laser (Tsunami, Spectra Physics, Mountain View, CA, USA) tuned to 910 nm. The average power at the objective was set to 3 mW equivalent to an average intensity of ∼6 MW/cm^2. Appropriate filters in the detection path (2×LP800+LP750, Newport, Irvine, USA; BG39-3, Schott, Mainz, Germany) allowed to reliably discriminate the GFP fluorescence. The fluorescence was detected by a photon-counting avalanche diode (SPCM-AQR-141, EG&G, Dumberry, Canada) in combination with an interface card (PMS300, Becker and Hickl, Berlin, Germany). The dwell time of the counter was set to 10 ms.

2.5. Electrophysiology

Single-channel patch-clamp recordings [19] were obtained with a List L/M EPC 7 amplifier from successfully transfected tsA201 cells. Ba^{2+} currents through single Ca^{2+} channels were recorded in the cell-attached configuration according to [20]. The dihydropyridine Ca^{2+} channel activator (−)-BAYK 8644 (2.5 μM) was included in the pipette solution to facilitate channel activity in the cell-attached configuration. This allowed for correct estimation of the number of channels in the patch. Pipettes (GC150F-7.5F) were fabricated from borosilicate glass (Clark Medical Instruments, Pangbourne, UK) and had resistances of 4–6 MΩ. Sigmacote was used to reduce pipette capacitance. Single-channel currents of the channels were evoked by repetitive depolarizations (0.66 Hz) applied for 0.480 s from a holding potential of −80 to 0 mV ($\alpha_{1C,77}$) and 10 mV ($\alpha_{1C,86}$, $\alpha_{1C,77K}$ and $\alpha_{1C,77L}$). Single-channel traces were filtered at 1 kHz and digitized at 4 kHz. All experiments were performed at room temperature.

2.6. Analysis of electrophysiological data

Single channel current amplitudes were determined by analyzing all point amplitude histograms fitted by Gaussian curves employing pClamp 6.0.3 software. Estimation of Ca^{2+} channel activity was primarily based on determination of overall channel open probability (P). P was calculated from the time course of mean channel activity N_p (N is the total number of channels; [21]) determined for each depolarizing voltage pulse defined as a sweep, and obtained by averaging all N_p values divided by the number of channels in the patch. The number of channels N was estimated by the method described in [22]. Channel availability (P_s) and open probability (P_o) according to $P = P_s \cdot P_o$ were calculated in multi-channel experiments employing a recently developed analysis method [20,22,23]. P_s was defined by the ratio (×100 in %) of depolarizing sweeps with channel activity to the total number of sweeps, and P_o represents a channel's open probability in non-blank sweeps. Open times were determined from non-overlapping channel openings [20]. Since P_o was usually $< 10\%$ and $N \leq 3$ in experiments used for open times analysis, open time distributions are expected not to be biased. Distributions were corrected for missed events by excluding events < 1 ms [20]. Open times histograms were fitted with multiexponential functions employing a Chebyshev fitting routine from pClamp 8 software.

2.7. Statistics

Averaged results are presented as mean ± S.E.M. for the number of experiments usually given in parentheses. Two-tailed t-test was used for statistical comparison considering differences statistically significant at $P < 0.05$.

3. Results

The human Ca^{2+} channel isoforms $\alpha_{1C,77}$ and $\alpha_{1C,86}$ (Table 1) were transiently co-expressed with β_{2a} and $\alpha_2\delta$ subunits in HEK-tsA201 cells. The expression pattern of these channels and electrophysiological properties of their single-channel currents were analyzed to characterize the functional role of the sequence 1572–1651. To narrow structures within the sequence 1572–1651 critical for functional properties, two segmental mutants, i.e. $\alpha_{1C,77L}$ and $\alpha_{1C,77K}$, were studied in which

Table 1
Structure of the variable parts in the carboxy-terminal tail of the investigated α_{1C} subunits

$\alpha_{1C,77}$	IKTEGNLE**Q**ANEELRAIIKKIW**K**RTSM**K**LLDQVVPPAGDDEV**T**VGKFY**A**TF**L**-I**Q**EYF**R**KFKKRKEQGLVGKPSQRNA**L**SL	(1572-1651)
$\alpha_{1C,77L}$	ETELSSQV**Q**YQAKEASLLERRR**K**SSHP	(1572-1598)
$\alpha_{1C,77K}$	SSHP**K**SSTKPNKLLSSGGS**T**GWVED**A**RA**L**EG**Q**VLA**R**GCGWLGSLEERERGPHHPP**L**GF	(1595-1652)
$\alpha_{1C,86}$	ETELSSQV**Q**YQAKEASLLERRR**K**SSHP**K**SSTKPNKLLSSGGS**T**GWVED**A**RA**L**EG**Q**VLA**R**GCGWLGSLEERERGPHHPP**L**GF	(1572-1652)

Amino acid sequences of $\alpha_{1C,77}$ (1572–1651) and $\alpha_{1C,86}$ (1572–1652) are shown on the top and bottom, respectively. Indicated amino acids of $\alpha_{1C,86}$ replace the respective residues in the amino acid sequence of $\alpha_{1C,77}$. In $\alpha_{1C,77L}$ and $\alpha_{1C,77K}$ subunits, indicated segments of $\alpha_{1C,86}$ replace the respective motifs L (1572–1598) and K (1595–1651) of the $\alpha_{1C,77}$ subunit. Note that the overlapping 4-amino acid segment SSHP has been proven not to contribute to the kinetics, voltage- or Ca^{2+}-dependence of inactivation ([11]). Bold residues are located in identical positions between α_{1C} subunits.

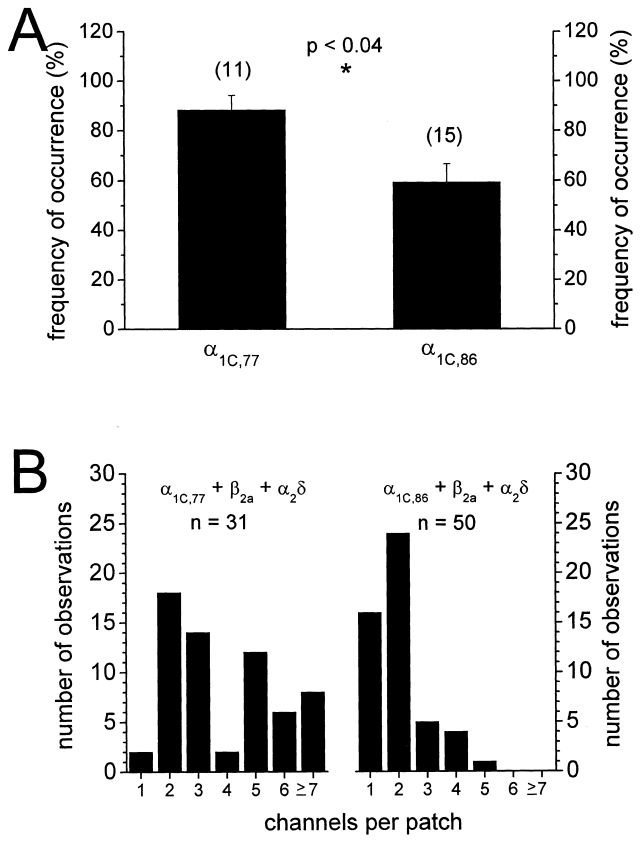

Fig. 1. Expression of the $\alpha_{1C,77}$ and $\alpha_{1C,86}$ channels in HEK-tsA201 cells. A: Frequency of occurrence of $\alpha_{1C,77}$ and $\alpha_{1C,86}$ channel activity in cell-attached patches estimated from day by day statistics. Transiently transfected tsA201 cells were selected on the basis of bound (>6) beads which carry antibodies against the co-expressed CD8 receptor. B: Number of cell-attached channel recordings with the respective number of channels in the patch.

segments of 27 (L) and 58 (K) amino acids, respectively, of $\alpha_{1C,86}$ replace the corresponding residues in the 80-amino acid sequence of $\alpha_{1C,77}$ (Table 1).

3.1. Subcellular targeting of $\alpha_{1C,77}$ and $\alpha_{1C,86}$ channels in tsA201 cells

In the electrophysiological experiments, a distinct behavior regarding the occurrence of $\alpha_{1C,77}$ and $\alpha_{1C,86}$ channels in the plasma membrane became obvious (Fig. 1). We found a significantly higher percentage of cells which exhibited channel activity in the cell-attached patch when expressing $\alpha_{1C,77}$ as compared to the $\alpha_{1C,86}$ channel (Fig. 1A). Furthermore, channel density evaluated from the number of overlapping channel openings in cell-attached patches (Fig. 1B) was larger with the $\alpha_{1C,77}$ channel suggesting more efficient targeting to the plasma membrane. This finding was substantiated by using fluorescent α_{1C} subunits that were labeled at their amino-termini by GFP (Table 2 and Fig. 2). In accordance with results obtained with homologous channels [24,25], N-terminal GFP-labeling of $\alpha_{1C,77}$ and $\alpha_{1C,86}$ did not significantly affect Ca^{2+} channel function in both whole-cell and single-channel experiments (data not shown). Conventional fluorescence microscopy revealed a different pattern of subcellular distribution for the GFP-labeled $\alpha_{1C,77}$ and $\alpha_{1C,86}$ subunits, when co-expressed with $\alpha_2\delta$ and β_{2a} subunits (Table 2). The $\alpha_{1C,77}$ subunit was mainly located in the plasma membrane with the formation of punctate clusters visible in 16% of these cells. In contrast, the $\alpha_{1C,86}$ subunit showed mainly cytoplasmic localization besides some plasma membrane staining without any indication of cluster formation. Fig. 2 shows two-photon confocal fluorescence images of equatorial slices through the α_{1C}-expressing tsA201 cells which illustrate the typical patterns of subcellular distribution as observed also in the conventional fluorescence microscopy. The fluorescence is attributed to GFP-labeled proteins as confirmed by images of cells transfected with non-fluorescent subunits (Fig. 2A). As control for plasma membrane localization, expression of the GFP-labeled pleckstrin homology (PH) domain that has been found to be enriched in the plasma membrane [26] is shown (Fig. 2B). The difference in cellular localization between $\alpha_{1C,77}$ and $\alpha_{1C,86}$ as given in Table 2 is clearly evident from comparison of Fig. 2C,D. Expression of each α_{1C} subunit alone resulted in similar expression patterns showing mainly intracellular localization (data not shown).

3.2. Single-channel characteristics of $\alpha_{1C,77}$ and $\alpha_{1C,86}$ channels

Single-channel currents were measured in the cell-attached configuration with Ba^{2+} as charge carrier in the presence of 2.5 μM (−)-BAYK 8644. Fig. 3A and B depict consecutive single-channel traces with corresponding ensemble average currents of $\alpha_{1C,77}$ and $\alpha_{1C,86}$, respectively. Consistent with whole-cell characteristics (data not shown; [10]), the ensemble average currents of $\alpha_{1C,86}$ showed a markedly faster inactivation rate as compared to the $\alpha_{1C,77}$ channel. Surprisingly, current–voltage relationships revealed a significantly lower single-channel Ba^{2+} conductance for the $\alpha_{1C,86}$ channel (Fig. 3C). A unitary conductance of 25.5 ± 0.8 pS ($n = 14$) was determined for $\alpha_{1C,86}$, whereas 29.3 ± 1.1 pS ($n = 5$) was calculated for the $\alpha_{1C,77}$ channel. Reversal potentials, however, did not significantly differ between these channels (Fig. 3C, inset) yielding 51.5 ± 4.1 and 57.8 ± 2.4 mV for $\alpha_{1C,77}$ and $\alpha_{1C,86}$, respectively.

To further evaluate the impact of the sequence 1572–1651 on Ca^{2+} channel gating characteristics, overall open probability (P) which is the product of open probability (P_o) times

Table 2
Comparison of the subcellular distribution of 5′-GFP-$\alpha_{1C,77}$ and 5′-GFP-$\alpha_{1C,86}$ in transfected tsA201 cells

α_{1C} subunits	Subcellular distribution		
	Mainly cytoplasmic	Mainly plasma membrane	n
5′-GFP-$\alpha_{1C,77}$	24%	76% 16% of these cells show punctate staining	250
5′-GFP-$\alpha_{1C,86}$	70%	30%	239

Numbers give percentage of cells in each category (n, total number of cells inspected). Shown are results obtained from five transfections of 5′-GFP-$\alpha_{1C,77}$, and seven transfections of 5′-GFP-$\alpha_{1C,86}$, both together with $\alpha_2\delta$ and β_{2a} subunits in tsA201 cells. Patterns of cell staining were inspected by eye using an inverted fluorescence microscope with 100× magnification (see Section 2).

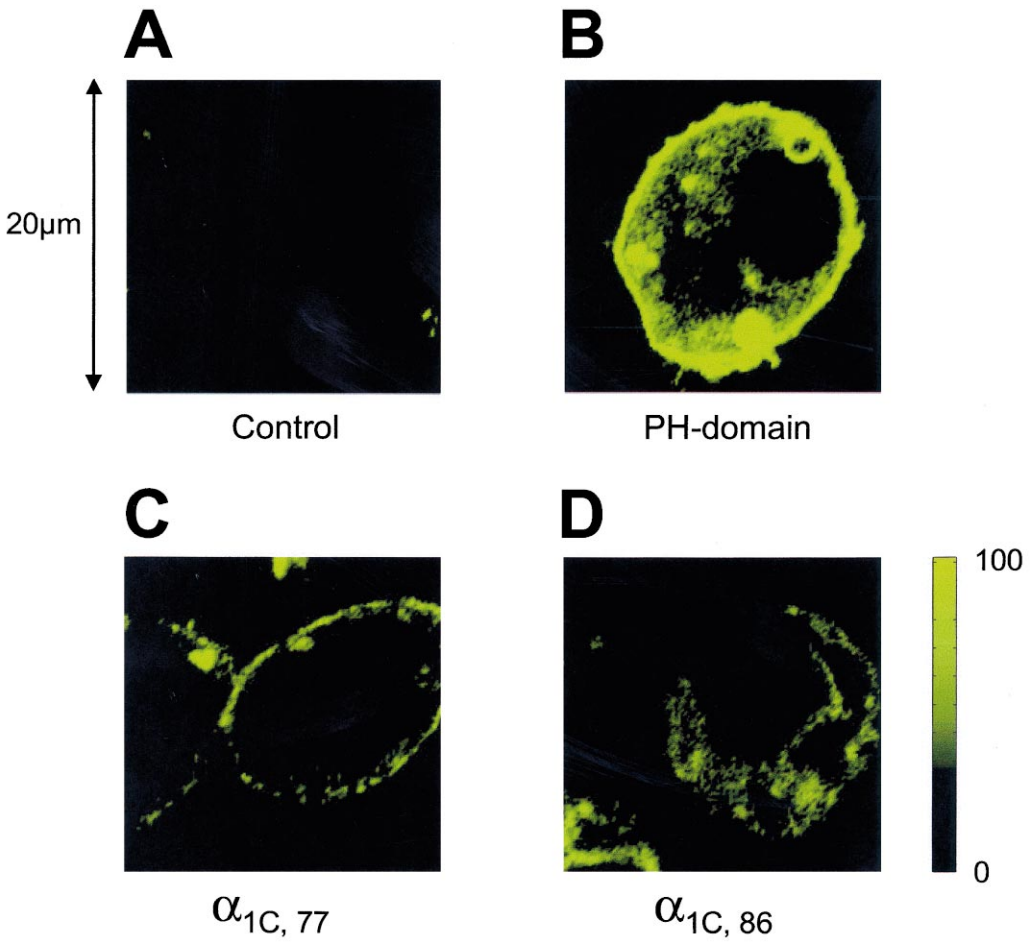

Fig. 2. Subcellular distribution of GFP-labeled proteins in tsA201 cells detected with two-photon confocal microscopy. tsA201 cells expressing (A) non-labeled subunits, (B) the GFP-labeled pleckstrin-homology (PH) domain, and the GFP-labeled (C) $\alpha_{1C,77}$ and (D) $\alpha_{1C,86}$ subunits both co-expressed with $\alpha_2\delta$ and β_{2a} subunits.

availability (P_S) were determined separately, and mean open times were estimated to reveal their contribution to the inactivation of channels (Fig. 4). It was found that P of $\alpha_{1C,77}$ was about 4-fold higher than that of the $\alpha_{1C,86}$ channel (Fig. 4A) This significant difference in P was mainly due to divergent P_o, whereas P_S was not changed between the channels (Fig. 4B). To evaluate whether inactivation visible in ensemble average currents is mediated by a reduction in open times with progressive depolarization time, we performed separate analysis of open time distributions (Fig. 4C,D) restricted to 0–240 and 241–480 ms of depolarization. Open time distributions of both channels were fitted by two exponentials suggesting the existence of at least two distinct open states which apparently do not significantly change with time. The short open time constant and the proportion between short and long open time constants were rather similar for both channels. However, the long open time constant was almost 1.5-fold greater for $\alpha_{1C,77}$ as compared to the $\alpha_{1C,86}$ channel. The average mean open times of both channels (see Table 3) within the first and second time interval of depolarization did not significantly change suggesting an increase in average mean closed times to account for the increase in inactivation rate of $\alpha_{1C,86}$.

To further narrow critical regions within the sequence 1572–1651 that appears to be important for the functional properties characterized above, single-channel characteristics of the two segmental mutants $\alpha_{1C,77L}$ and $\alpha_{1C,77K}$ were studied.

3.3. *Single-channel characteristics of the segmental mutants $\alpha_{1C,77K}$ and $\alpha_{1C,77L}$*

Single-channel characteristics of $\alpha_{1C,77K}$ and $\alpha_{1C,77L}$ channels are shown in Figs. 5 and 6, and summarized in Table 3. Consecutive current traces and their corresponding ensemble average currents (Fig. 5A,B) reflect the rapid inactivation observed in whole-cell currents (data not shown; [11]). Analysis of single-channel current–voltage relationships for $\alpha_{1C,77K}$ and $\alpha_{1C,77L}$ channels showed no significant difference either in their reversal potentials or in unitary conductances (Fig. 5C). Their conductances were also not significantly different to the $\alpha_{1C,86}$ channel, but were clearly distinct to that of the $\alpha_{1C,77}$ channel. Analysis of single-channel gating kinetics (Fig. 6) revealed that P of $\alpha_{1C,77K}$ and $\alpha_{1C,77L}$ (Fig. 6A) amounted on the average to $1.3 \pm 0.4\%$ ($n = 10$) and $2.3 \pm 1.1\%$ ($n = 8$) and were estimated to be not significantly different. Consistently, both P_S and P_o of the $\alpha_{1C,77K}$ and $\alpha_{1C,77L}$ channel were not significantly different (Fig. 6B). However, the time-restricted open time analysis (Fig. 6C) revealed a substantial reduction in mean open times of α_{1C77K} with increasing depolarization time, which was not found with the $\alpha_{1C,77L}$ channel.

4. Discussion

In this study, we characterized functional expression of the human L-type Ca^{2+} channel splice variants $\alpha_{1C,77}$ and $\alpha_{1C,86}$ as well as their segmental mutants $\alpha_{1C,77K}$ and $\alpha_{1C,77L}$. Our results strongly suggest that the sequence 1572–1651 in the carboxy-terminal tail of α_{1C} is critical for subcellular protein targeting and significantly affects single-channel conductance and gating of L-type Ca^{2+} channels (summarized in Table 3).

4.1. Expression and subcellular localization pattern of splice variants

Estimation of Ca^{2+} channel density in transfected tsA201 cells points to stronger expression of the $\alpha_{1C,77}$ channel as compared to $\alpha_{1C,86}$. Consistently, we observed a different pattern of subcellular distribution for these splice variants using fluorescent α_{1C} subunits. The GFP-$\alpha_{1C,77}$ subunit, when expressed together with auxiliary subunits, was mainly localized in the plasma membrane, and in 16% of cells formed clusters, whereas the $\alpha_{1C,86}$ subunit was detected predominantly in the cytoplasm. This distinct expression pattern did not change with time between the first and third day after transfection

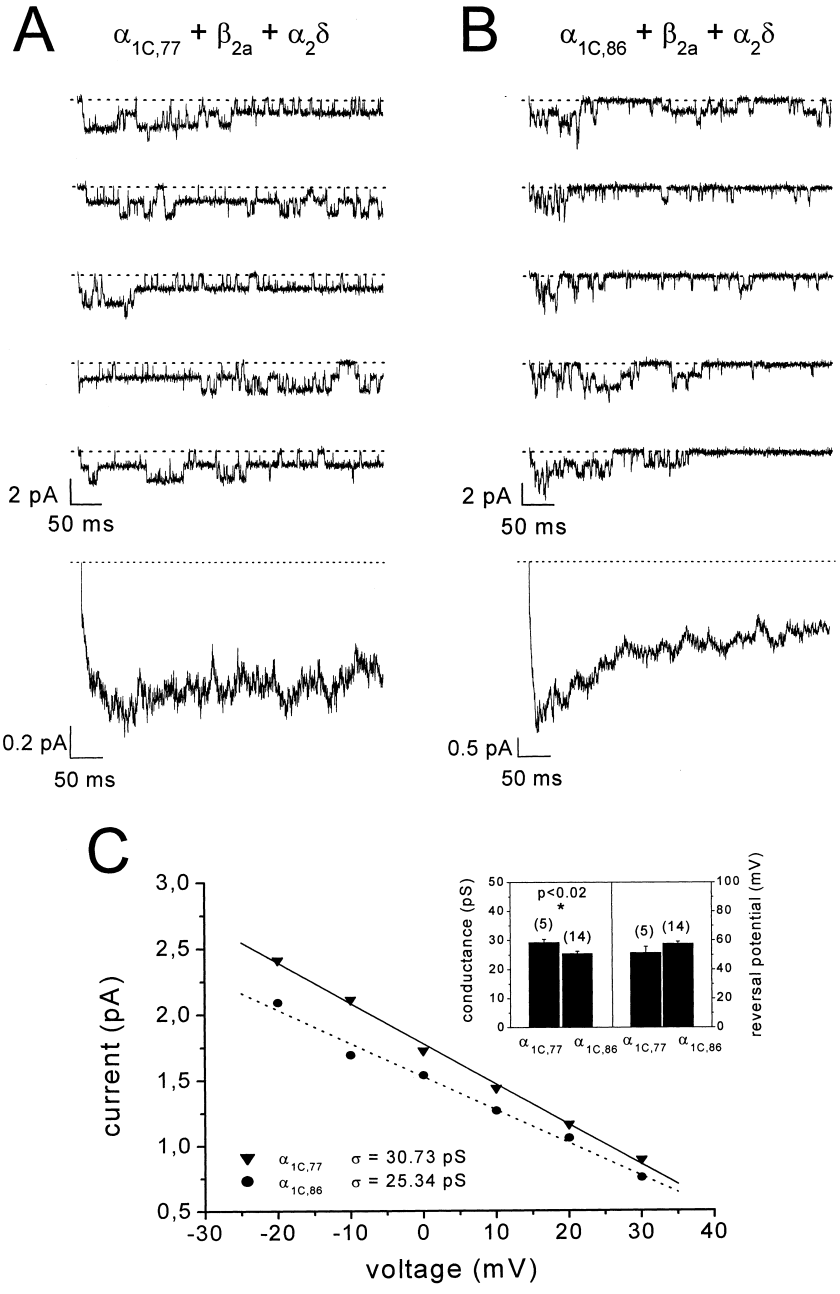

Fig. 3. Single-channel characteristics of the $\alpha_{1C,77}$ and $\alpha_{1C,86}$ channels. Single-channel traces obtained from (A) $\alpha_{1C,77}$ and (B) $\alpha_{1C,86}$ channels by repetitive depolarizations (0.66 Hz) from a holding potential of −80 to 0 and 10 mV, respectively. Corresponding average currents are shown at the bottom of A and B. Dotted lines indicate zero current level. C: Corresponding current–voltage relationships of typical experiments with unitary conductance (σ) as indicated. Inset in C depicts respective mean values showing a significant difference ($P < 0.02$) between unitary conductances of the $\alpha_{1C,77}$ and $\alpha_{1C,86}$ channels, but not in their reversal potentials.

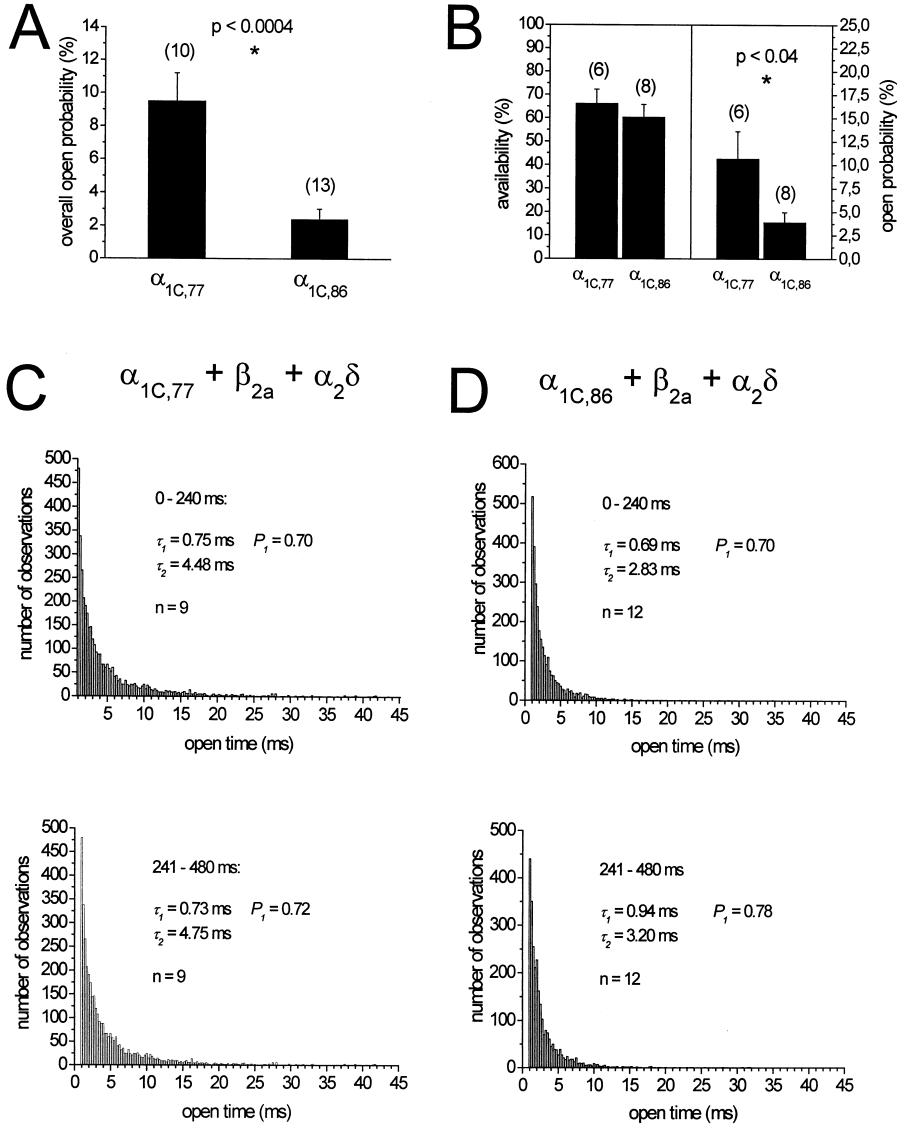

Fig. 4. Gating characteristics of single $\alpha_{1C,77}$ and $\alpha_{1C,86}$ channels. (A) Overall open probability and (B) availability as well as open probability of the respective channel. Numbers of experiments are indicated in parentheses and significant differences are marked by an asterisk. Open time histograms of (C) $\alpha_{1C,77}$ and (D) $\alpha_{1C,86}$ channels constructed from the indicated number (n) of experiments for the first (0–240 ms) and second (241–480 ms) time interval of depolarizations. Open times (τ) and proportions (P) were calculated from the respective biexponential open time distributions fitted by a Chebyshev algorithm.

(data not shown). Hence, targeting of the $\alpha_{1C,86}$ subunit to the plasma membrane appears to be less efficient. Previously, the targeting of α_{1C} subunit to plasma membrane has been demonstrated to be critically dependent on the interaction with the β subunit [25,27–29]. Accordingly, in the absence of β_{2a}, both $\alpha_{1C,77}$ and $\alpha_{1C,86}$ subunits were diffusely distributed in the cytoplasm (data not shown). The interaction with the β subunit, however, is expected to be similar for $\alpha_{1C,77}$ and $\alpha_{1C,86}$, as both subunits retain invariant β-subunit binding domain in the cytoplasmic linker between repeats I and II of the core protein. Our results are consistent with the idea that the carboxyl tail of the conventional $\alpha_{1C,77}$ channel contains additional structures critical for membrane targeting that appear to be disrupted in $\alpha_{1C,86}$. Furthermore, the segmental mutants $\alpha_{1C,77K}$ and $\alpha_{1C,77L}$ exhibited an expression pattern which resembles that of $\alpha_{1C,86}$ (data not shown). Recent data supporting our findings suggest that the C-terminus of the α_{1C} subunit is required for proper plasma membrane targeting of L-type Ca^{2+} channels ([30]; B. Flucher, personal communication). Our study allowed this additional critical structure to be narrowed to the 80-amino acid motif 1572–1651 at the α_{1C} tail.

4.2. *Electrophysiological features of α_{1C} splice variants and segmental mutants in single-channel experiments*

The $\alpha_{1C,77}$ channel exhibited a significantly slower inactivation than $\alpha_{1C,86}$ and the two segmental mutants $\alpha_{1C,77K}$ and $\alpha_{1C,77L}$, as judged from ensemble average currents. These data substantiated the role of the sequence 1572–1651 and of its L- and K-segments (see Table 1) as molecular determinants of voltage-dependent inactivation [11]. In addition, current–voltage relationships implied the sequence 1572–1651 as affecting the unitary conductance. The three α_{1C} channel isoforms which exhibited rapid inactivation of Ba^{2+} currents showed

a significantly lower single-channel conductance compared to the $\alpha_{1C,77}$ channel. We discovered that substitution of segment L (1572–1598) or K (1595–1651) in $\alpha_{1C,77}$ by the corresponding sequences of the $\alpha_{1C,86}$ subunit was sufficient to reduce unitary conductance of the resulting $\alpha_{1C,77L}$ and $\alpha_{1C,77K}$, respectively, channels to almost the same level as that seen in the $\alpha_{1C,86}$ channel. This finding was unexpected, as the pore-structure remains identical in all channels studied which is consistent with no significant difference in their reversal potentials. The fact that each of the two adjacent cytoplasmic motifs K and L of the $\alpha_{1C,86}$ tail reduced unitary conductance to the same level seen in the $\alpha_{1C,86}$ channel suggests that there are two independent determinants for this effect. In view of recent results obtained with a Shaker channel [31], a link between cytoplasmic domains and permeation properties appears possible. However, the sequence 1572–1651 is not a critical determinant of permeation, as its deletion still yields functional channels [32], but rather has a modulatory role.

4.3. Molecular determinants of gating kinetics

The 4–7-fold lower P of the $\alpha_{1C,86}$ channel and of its segmental mutants $\alpha_{1C,77K}$ and $\alpha_{1C,77L}$ compared to the $\alpha_{1C,77}$ channel is mediated by a decrease in P_o, whereas P_S is not significantly changed. As (−)-BAYK 8644 was used in all

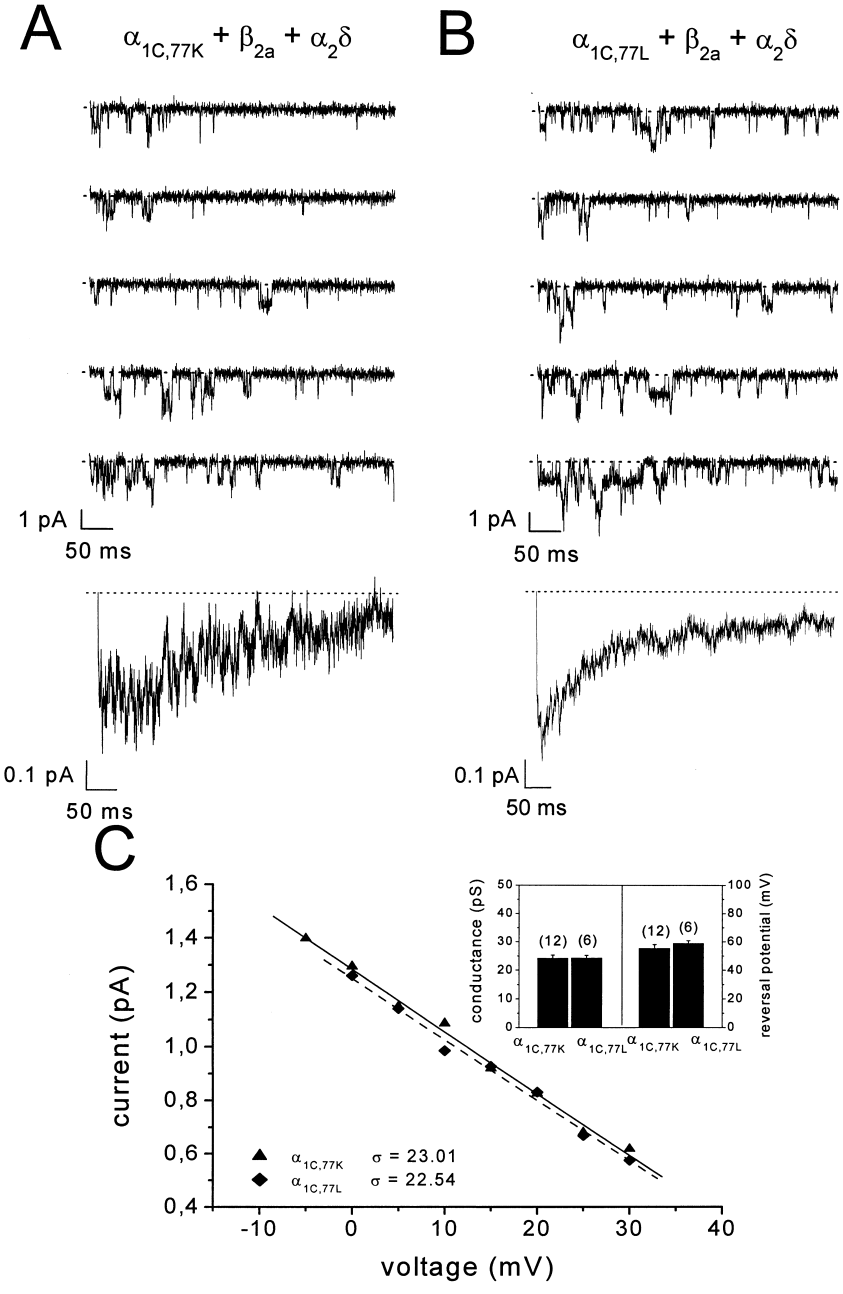

Fig. 5. Single-channel characteristics of single $\alpha_{1C,77K}$ and $\alpha_{1C,77L}$ channels. Single-channel traces of (A) $\alpha_{1C,77K}$ and (B) $\alpha_{1C,77L}$ channels recorded by repetitive depolarizations (0.66 Hz) from a holding potential of −80 to 10 mV. Corresponding average currents are shown at the bottom of A and B. Dotted lines denote zero current level. C: Corresponding current–voltage relationships of typical experiments are shown with estimated unitary conductances (σ) and reversal potentials (E_{rev}) as indicated. Inset depicts respective mean values showing no significant difference between both unitary conductances and reversal potentials of $\alpha_{1C,77K}$ and $\alpha_{1C,77L}$ channels.

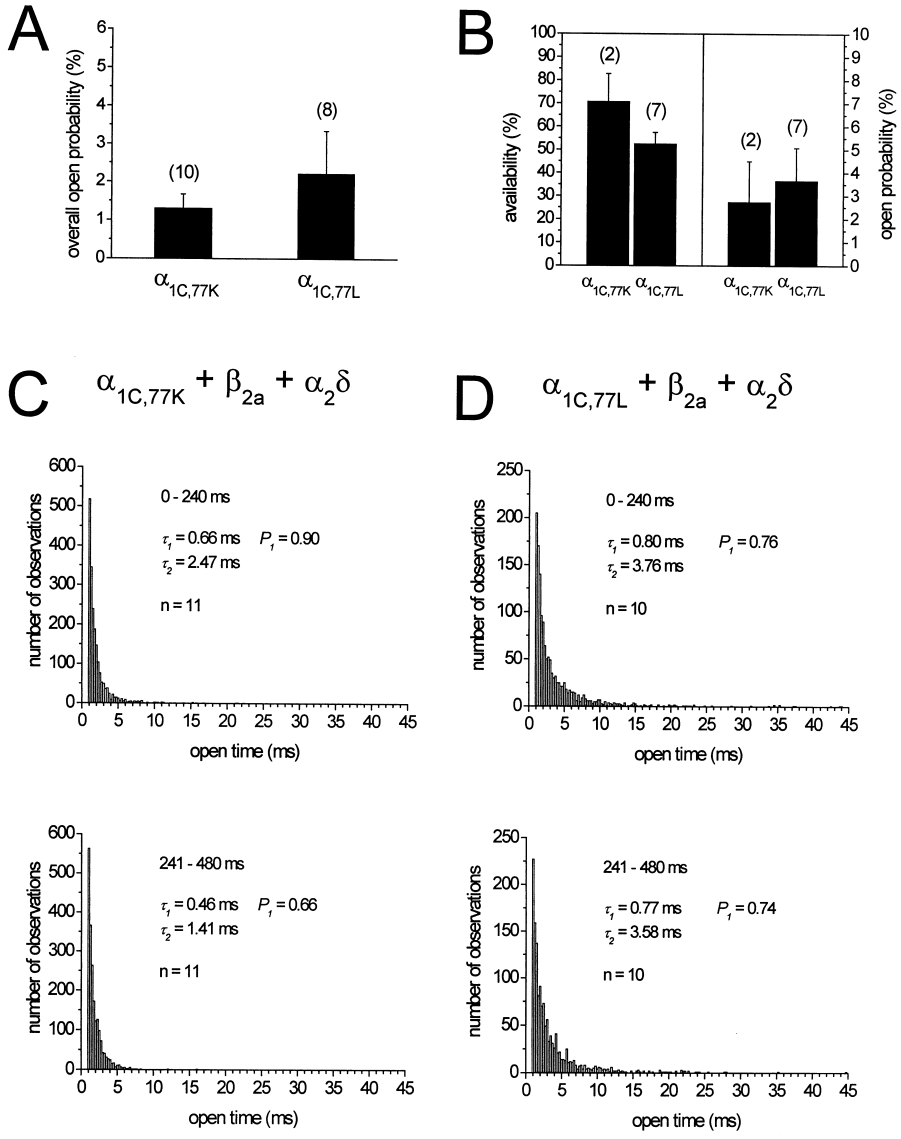

Fig. 6. Gating characteristics of single $\alpha_{1C,77K}$ and $\alpha_{1C,77L}$ channels. (A) Overall open probability and (B) availability as well as open probability of the respective channel. Numbers of experiments are indicated in parentheses. Open time histograms of (C) $\alpha_{1C,77K}$ and (D) $\alpha_{1C,77L}$ channels constructed from the indicated number (n) of experiments for the first (0–240 ms) and second (241–480 ms) time interval of depolarizations. Open times (τ) and proportions (P) were calculated from the respective biexponential open time distributions fitted by a Chebyshev algorithm.

experiments, the difference in P_o could be at least in part due to different affinities of the channels to dihydropyridines [33]. To largely compensate for these different affinities to (−)-BAYK 8644, supramaximal concentrations of 2.5 μM (−)-BAYK 8644 were used. Hence, the sequence 1572–1651 appears to determine P_o of the Ca^{2+} channel. In accordance, Ca^{2+}-induced inactivation of the channel, which critically depends on this sequence [10], is manifested in a reduction of P_o while leaving P_S unchanged [20].

To evaluate the impact of the sequence 1572–1651 on chan-

Table 3
Overview of the investigated properties of the $\alpha_{1C,77}$ and $\alpha_{1C,86}$ channels and their segmental mutants $\alpha_{1C,77K}$ and $\alpha_{1C,77L}$

α_{1C}	Subcellular localization	Ba^{2+} current inactivation	σ(pS)	E_{rev} (mV)	P_s (%)	P_o (%)	τ_{mean} (ms) 0–240 ms	τ_{mean} (ms) 241–480 ms
77	mainly plasma membrane	slow	29.3 ± 1.1	51.5 ± 4.1	66.3 ± 6.0	10.7 ± 2.9	1.87	1.86
86	mainly cytoplasm	rapid	25.5 ± 0.8	57.8 ± 1.3	60.4 ± 5.3	3.9 ± 1.0	1.33	1.44
77K	mainly cytoplasm	rapid	24.2 ± 1.1	55.3 ± 2.8	70.8 ± 11.9	2.7 ± 1.8	0.84	0.79
77L	mainly cytoplasm.	rapid	24.3 ± 1.0	58.9 ± 1.9	52.5 ± 4.9	3.7 ± 1.4	1.51	1.50

Subcellular localization has been assessed using 5′-GFP-labeled α_{1C} subunits; σ unitary conductance in 96 mM Ba^{2+}; E_{rev}, reversal potential; P_S, channel availability; P_o, channel open probability; τ_{mean}, mean open times within 0–240 ms and 241–480 ms intervals of depolarization time.

nel inactivation, open time histograms were constructed for 0–240 and 241–480 ms time intervals of the depolarizing pulse. Both $\alpha_{1C,77}$ and $\alpha_{1C,86}$ as well as the segmental mutants $\alpha_{1C,77L}$ and $\alpha_{1C,77K}$ yielded open time histograms that implied two open states. Mean open times within the first and the second interval are rather similar (see Table 3) pointing to an increase in mean closed times to account for the faster inactivation rate of $\alpha_{1C,86}$ and its segmental mutants $\alpha_{1C,77K}$ and $\alpha_{1C,77L}$. Only the $\alpha_{1C,77K}$ channel showed a clear reduction in open times during the 241–480 ms time interval, which is, however, balanced by a concomitant change in the proportion between these open times.

In summary, the amino acid sequence 1572–1651 in the carboxy-terminal tail of the human α_{1C} subunit not only determines voltage- and Ca^{2+}-dependent inactivation, but, in addition, represents a key structure for L-type Ca^{2+} channel membrane targeting, ion conductance and kinetics. The motifs K and L are independently critical for unitary conductance and open probability.

Acknowledgements: We thank N. Klugbauer, F. Hofmann (Munich) and V. Flockerzi (Heidelberg) for a gift of clones of β_{2a} and $\alpha_2\delta$ subunits. This work was supported by the Austrian Science Foundation P12803 to T.S., P12728 to C.R., Austrian Ministry of Science, project GC 200.027/3 to H.S., SFB Biomembranes F715 and P12667 to K.G., NB 7000 to C.R. and NIA, NIH to N.M.S. We wish to thank Mrs. Sabine Buchegger, Ingrid Gegenleitner and Bettina Kenda for their excellent technical assistance.

References

[1] Fabiato, A. and Fabiato, F. (1979) Annu. Rev. Physiol. 41, 473–484.
[2] Rios, E. and Brum, G. (1987) Nature 325, 717–720.
[3] Sheng, M., McFadden, G. and Greenberg, M.E. (1990) Neuron 4, 571–582.
[4] Murphy, T.H., Worley, P.F. and Barbaran, J.M. (1991) Neuron 7, 625–635.
[5] Deisseroth, K., Bito, H. and Tsien, R.W. (1996) Neuron 16, 89–101.
[6] Deisseroth, K., Heist, E.K. and Tsien, R.W. (1998) Nature 392, 198–202.
[7] Hofmann, F., Biel, M. and Flockerzi, V. (1994) Annu. Rev. Neurosci. 17, 399–418.
[8] Catterall, W.A. (1995) Annu. Rev. Biochem. 64, 493–531.
[9] Schultz, D., Mikala, G., Yatani, A., Engle, D.B., Iles, D.E., Segers, B., Sinke, R.J., Weghuis, D.O., Klockner, U. and Wakamori, M. (1993) Proc. Natl. Acad. Sci. USA 90, 6228–6232.
[10] Soldatov, N.M., Zühlke, R.D., Bouron, A. and Reuter, H. (1997) J. Biol. Chem. 272, 3560–3566.
[11] Soldatov, N.M., Oz, M., O'Brien, K.A., Abernethy, D.R. and Morad, M. (1998) J. Biol. Chem. 273, 957–963.
[12] Soldatov, N.M. (1992) Proc. Natl. Acad. Sci. USA 89, 4628–4632.
[13] Soldatov, N.M. (1994) Genomics 22, 77–87.
[14] Peterson, B.Z., DeMaria, C.D. and Yue, D.T. (1999) Neuron 22, 549–558.
[15] Zühlke, R.D., Pitt, G.S., Deisseroth, K., Tsien, R.W. and Reuter, H. (1999) Nature 399, 159–162.
[16] Qin, N., Olcese, R., Bransby, M., Lin, T. and Birnbaumer, L. (1999) Proc. Natl. Acad. Sci. USA 96, 2435–2438.
[17] Soldatov, N.M., Bouron, A. and Reuter, H. (1995) J. Biol. Chem. 270, 10540–10543.
[18] Denk, W., Strickler, J.H. and Webb, W.W. (1990) Science 248, 73–76.
[19] Hamill, O.P., Marty, A., Neher, E., Sakmann, B. and Sigworth, F.J. (1981) Pflügers Arch. 391, 85–100.
[20] Höfer, G.F., Hohentanner, K., Baumgartner, W., Groschner, K., Klugbauer, N., Hofmann, F. and Romanin, C. (1997) Biophys. J. 73, 1857–1865.
[21] Seydl, K., Karlsson, J.O., Dominik, A., Gruber, H. and Romanin, C. (1995) Pflügers Arch. 429, 503–510.
[22] Baumgartner, W., Hohentanner, K., Höfer, G.F., Groschner, K. and Romanin, C. (1997) Biophys. J. 72, 1143–1152.
[23] Schmid, R., Seydl, K., Baumgartner, W., Groschner, K. and Romanin, C. (1995) Biophys. J. 69, 1847–1857.
[24] Grabner, M., Dirksen, R.T. and Beam, K.G. (1998) Proc. Natl. Acad. Sci. USA 95, 1903–1908.
[25] Gerster, U., Neuhuber, B., Groschner, K. and Striessnig, J. (1999) J. Physiol. 517, 353–368.
[26] Stauffer, T.P., Ahn, S. and Meyer, T. (1998) Curr. Biol. 8, 343–346.
[27] Chien, A.J., Zhao, X., Shirokov, R.E., Puri, T.S., Chang, C.F., Sun, D., Rios, E. and Hosey, M.M. (1995) J. Biol. Chem. 270, 30036–30044.
[28] Yamaguchi, H., Hara, M., Strobeck, M., Fukasawa, K., Schwartz, A. and Varadi, G. (1998) J. Biol. Chem. 273, 19348–19356.
[29] Gao, T., Chien, A.J. and Hosey, M.M. (1999) J. Biol. Chem. 274, 2137–2144.
[30] Gao, T. and Hosey, M.M. (1999) Biophys. J. 76, A341.
[31] Kreusch, A., Pfaffinger, P.J., Stevens, C.F. and Choe, S. (1998) Nature 392, 945–948.
[32] Zühlke, R.D. and Reuter, H. (1998) Proc. Natl. Acad. Sci. USA 95, 3287–3294.
[33] Zühlke, R.D., Bouron, A., Soldatov, N.M. and Reuter, H. (1998) FEBS Lett. 427 (2), 220–224.